International Research Journal of Earth Sciences _____ ISSN 2321 – 2527
Vol. **7(2),** 13-26, May **(2019)** *Int. Res. J. Earth Sci.*

Geo-magnetic survey for estimating magnetic sources parameters by properties technique in Gol-e-Gohar area

Shekar Behnam* **and Hamidreza Ramazi**
[1]Department of Mining and Metallurgy, Amirkabir University of Technology (Tehran Polytechnic), 424 Hafez Ave, 15875-4413, Tehran, Iran
shkrbehnam@gmail.com

Available online at: www.isca.in
Received 29th November 2018, revised 15th April 2019, accepted 18th May 2019

Abstract

In the current research paper, the evaluation of magnetic data of Gol-e-Gohar Iron Ore Anomaly No. 8, located about 50km southwest of Sirjan, Kerman Province, was discussed. According to geological studies, the main minerals of the area constitute magnetite and hematite created from secondary oxidation. Acquired geomagnetic data was processed after applying diurnal and IGRF corrections (some unimportant corrections such as the topographic correction are eliminated). The results show two major anomalies including anomaly with the positive pole in the northern part and other anomaly with the northwest-southeast trending in the SE part. After initial studies the north trend anomaly was found to be insignificant. Further studies were done on the southeast anomaly. Several methods are reviewed and compared for estimating depth and a two-dimensional modeling is introduced to achieve a more precise method for achieving acceptable depth and tilt angle revealing the edge of the anomaly. Techniques and methods used to estimate the depth of sub-surface structures, include Euler Deconvolution, (Source Parameter Imaging) SPI, Werner Deconvolution, and Potentq two-dimensional modeling. These methods initially were applied to validate on two-dyke models. The results of applying synthetic models on the above-mentioned methods indicated that all of the above methods have the high accuracy for applying over the actual data. After applying to the data of the study area, all three methods provided similar results, however, considering the results of synthetic models and the measured data, it is indicated that the three-dimensional Euler Deconvolution method is the most appropriate method for estimating the depth. Therefore, applying these methods on actual data, the depth to an anomaly is determined 35 m in the center and the northeast of the mass and up to 50 m in the southeast part of body. It should be noted that the precision of the proposed methods depends on the shape and the source of the anomaly. The more ideal and simple and not affected by several sources the mass form is, the more accurate the answer will be.

Keywords: Iron, euler deconvolution, werner deconvolution, SPI, 2D modeling.

Introduction

Gol-e-Gohar iron ore deposits is located in southern of Iran, at 55 kilometers of southwest of the Sirjan (approximately 29°N, 55°E). Gol-e-Gohar iron ore with 8 distinct anomalies (1 to 8) within an area of approximately 10*4 km^2 is important reserves of iron ore in Iran and the Middle East. The main ore minerals are magnetite and hematite. In this study, quantitative and quantitative interpretation of quantitative magneto metric data of Number 8 Gol-e-Gohar area is considered. The purpose of the quantitative data interpretation is to obtain the information regarding the depths of the magnetic bodies, their size and shape, and their magnetic details. In this work, in addition to the magnetic field interpretation, it is attempted to find the most suitable method for estimating the depths among the methods used in this paper. This study was conducted through both the application of the mentioned methods on the synthetic models and the response of the actual data.

To obtain source depth information we employ three semi-automated depth estimation techniques: Euler deconvolution, Werner deconvolution and (SPI); and a potential field modeling procedures: discrete object modeling (Potent).

Source depth estimation techniques are used extensively to find the depth of magnetic sources in the absence of a priori information. Werner and Eulerdeconvolution are two of the more standard methods and have been in use for decades. Euler deconvolution is based on using Euler's homogeneity equation that solves an over determined set of linear equations using a least-squares routine. The equation requires that a SI (structural index) be declared for each source, ranging from 0 (contact), 1 (dyke), 2 (horizontal/vertical cylinder) and 3 (sphere) based on the fall-off rate of the field[1,2]. A solution search window designated by the interpreter isgenerally based on the width of the source. Werner deconvolution transforms a complex non-linear function magnetic inversion to a simple linear inversion to solve for location, geometry and depth[3]. Like Euler it also uses a moving window (Werner operator) and works for a contact and thin dyke. Both methods use only first derivatives so they are fairly resilient in the presence of noise. However each method can produce erroneous depth estimates where the

moving window incorporates interfering signal of broader or adjacent source anomalies.

SPI is a more recent method based on the full analytic signal by computing 3 complex attributes (amplitude, local phase and local frequency) from which source parameters can be computed[4,5]. Depth is calculated from the max of the local wavenumber. This approach works for SI's from 0 to 2. This method works on total field and gradient data, and is not dependent on a user selected window size.

Geological Setting

The current area is located in the eastern part of the Gol-e-Gohar Iron deposit and in the Sanandaj Sigran metamorphic-Magmatic Zone (Figure-1). Stratigraphy of Gol-e-Gohar and surrounding area is mostly covered by recent alluvium, and few Altitudes which are outcropped have Paleozoic metamorphic units in south and south west, Mesozoic-Cenozoic sedimentary units in east.

According to stratigraphy, the oldest rock units that outcrops in the study area are Gol-e-Gohar metamorphic complexes that consist of volcano-sedimentary sequences with the Upper Paleozoic-Mesozoic age that are covered by Cenozoic rock sequences. The magnetic bodies are hosted by a Paleozoic-Mesozoic sequence of gneisses, quartz-biotite schists, calc-schists, quartzites and amphibolites. In this area, the main minerals are magnetite, pyrite, pyrrhotite, chalcopyrite, pentlandite, sphalerite and minor apatite. The most important alterations are including sodic-calcic, potassic and phyllic. Alteration minerals such as olivine, actinolite, hornblende, phlogopite, chlorite and carbonates are associated with the Fe-oxide minerals[6].

Methods and Data

Field observations: For geomagnetic data surveying, a regular grid was designed which included 41 profiles with a distance of 40 meters and north-south trending which totally included 3156 points. Points intervals on each profile were considered around 20 meters. GPS devices were used to survey all these points for the coordinates. Geomagnetic data were surveyed by using proton magnetometer GSM19T model. The geomagnetic inclination and declination in the study area are 45.6 and 2.8 degrees, respectively.

Preliminary maps and Source edge detection: The detected anomalies on the residual map strongly fit to the features and specifications in the total intensity magnetic field map. Two main anomalies were detected, one is located in the north and another in southeast of the map (Figure-2a).

Indeed, because of the dipolar nature of geomagnetic field, magnetic sources observed anywhere except magnetic poles are asymmetric that this feature make difficult the interpretation of magnetic data. Reduce to the pole (RTP) technique is implemented over the TMI grid, in order to convert magnetic anomaly to symmetric shape that the angle of inclination is 90° and declination is zero where the effects of dipoles were eliminated. In the study area, RTP was applied to the diurnally corrected data (Figure-2b).

Total gradient map shows the boundaries of the ferromagnetic bodies and analytic signal helped highlight shallower features (high frequencies) and being based on the derivatives it will in fact have the opposite effect for better representation of the magnetic body. The north anomaly is almost unknown; however, the southeast anomaly is clearly visible on the map (Figure-2c). The anomaly located in the northern area which has a high surface extension and appeared in discontinuous unipolar form on the map, is not very significant.

By further studying the different analytic signal and vertical derivative maps, it was concluded that the anomaly is sporadically related to the rocks containing magnetic minerals with no sign of iron mineralization occurrence.

Therefore, for more precise and detailed studies we focused on the southeast anomalies.

Different processing methods are used to increment delicate specification in magnetic data, including upward continuation, derivatives filters, and other existing processes. Mr. Miller and Singh suggest using the tilt angle, namely the ratio of the vertical gradient to the total horizontal gradient[7]:

$$\mathrm{TDR} = \tan^{-1}\left(\frac{\frac{\partial \mathrm{f}}{\partial \mathrm{z}}}{\sqrt{\left(\frac{\partial \mathrm{f}}{\partial \mathrm{x}}\right)^2+\left(\frac{\partial \mathrm{f}}{\partial \mathrm{y}}\right)^2}}\right) \quad (1)$$

According to Figure-2d., the tilt angle value is positive over the magnetic body, and also is zero (close-by zero) and negative at the edge where the vertical derivative is zero and the horizontal derivative is a maximum and the outside of the body, respectively.

Mr. Verduzco et al. introduced the total horizontal derivative (THDR) as an edge detection filter[8]:

$$\mathrm{THDR} = \sqrt{\left(\frac{\partial \mathrm{T}}{\partial \mathrm{x}}\right)^2 + \left(\frac{\partial \mathrm{T}}{\partial \mathrm{y}}\right)^2} \quad (2)$$

The total horizontal derivative properly detects the edges of the high frequency anomalies (near surface bodies), but its outcomes for the subsurface anomalies are less accurate. As well as, it is a maximum over the edges of the magnetized source and it is independent of the geomagnetic field.

A prevalent thrust, fault, edge detector technique is the horizontal tilt angle method (TDX),

$$\mathrm{TDX} = \tan^{-1}\left(\frac{\mathrm{THDR}}{\left|\frac{\partial \mathrm{T}}{\partial \mathrm{z}}\right|}\right) \quad (3)$$

By applying TDX method, the edges of the anomalies are enhanced, and it responds well to deep bodies but the outcome is dominated by the response from the near surface source[9]. The result of total horizontal derivative is shown on the map (Figure-3).

Euler Deconvolution: Thompson initially used the Euler homogeneous equation for the two-dimensional interpretation of magnetic data as an automatic method[1]. After presenting Euler method by Thompson, Reid used this apraoch for the three-dimensional interpretation of magnetic data[2]. For an magnetic field, the Euler equation is written as the following:

$$(x - x_0)\frac{\partial T}{\partial x} + (y - y_0)\frac{\partial T}{\partial y} + (z - z_0)\frac{\partial T}{\partial z} = N(B - T) \qquad (4)$$

Where (x_0, y_0, z_0) is the magnetic body depth locations whose total field T is measured at a point (x,y,z). B is the regional value of the total field, and N expresses the change ratio of magnetic field with distance which takes different values for different magnetic source. N is directly related to the shape of sources (Table-1) that called the structural index (SI)[1]. Finally, a system of simultaneous equations is come from assessing the total field T and its three gradients (calculated or measured) at all points on a magnetic grid.

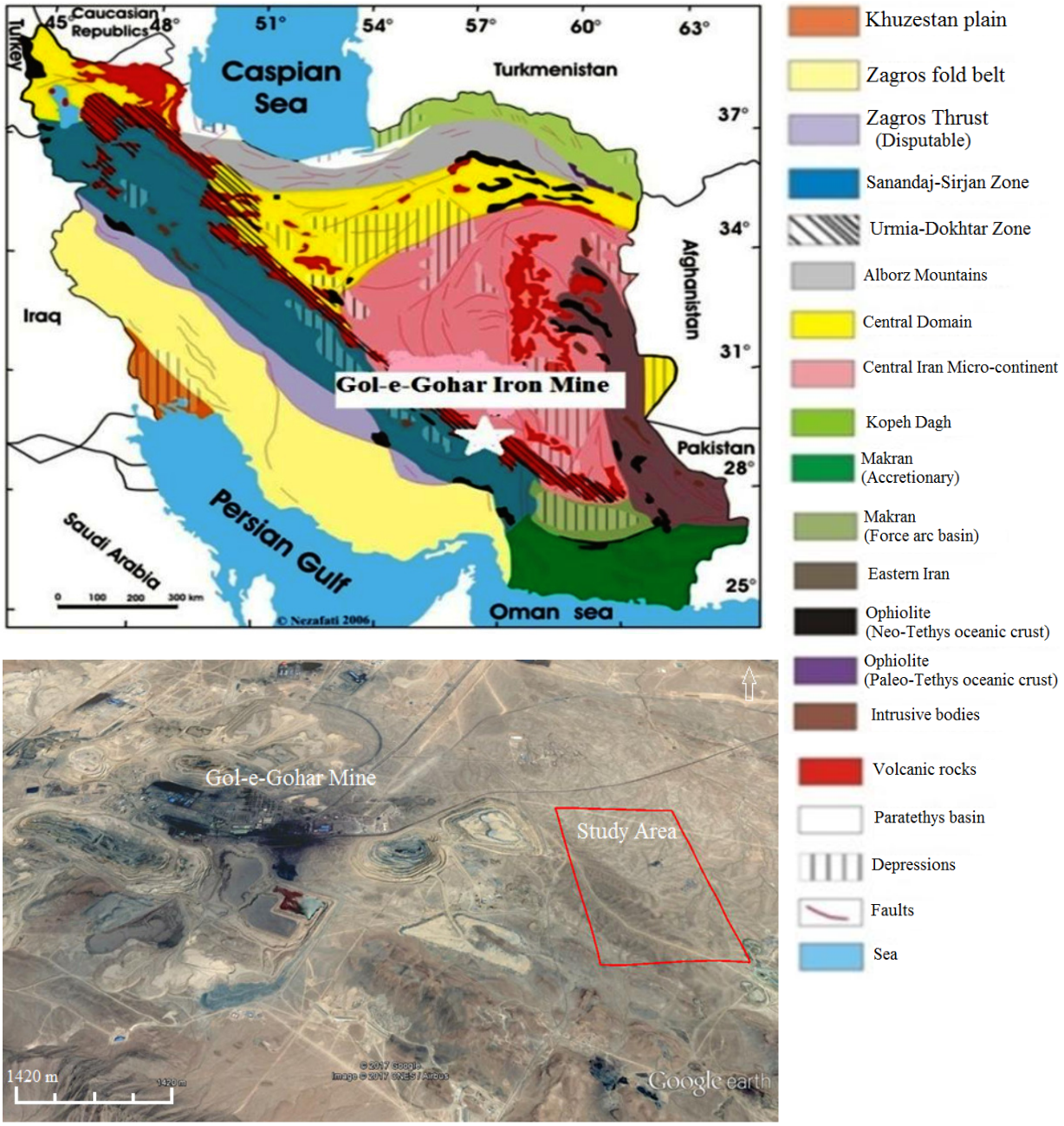

Figure-1: Location of the Gol-e-Gohar Mine and study region within Iran.

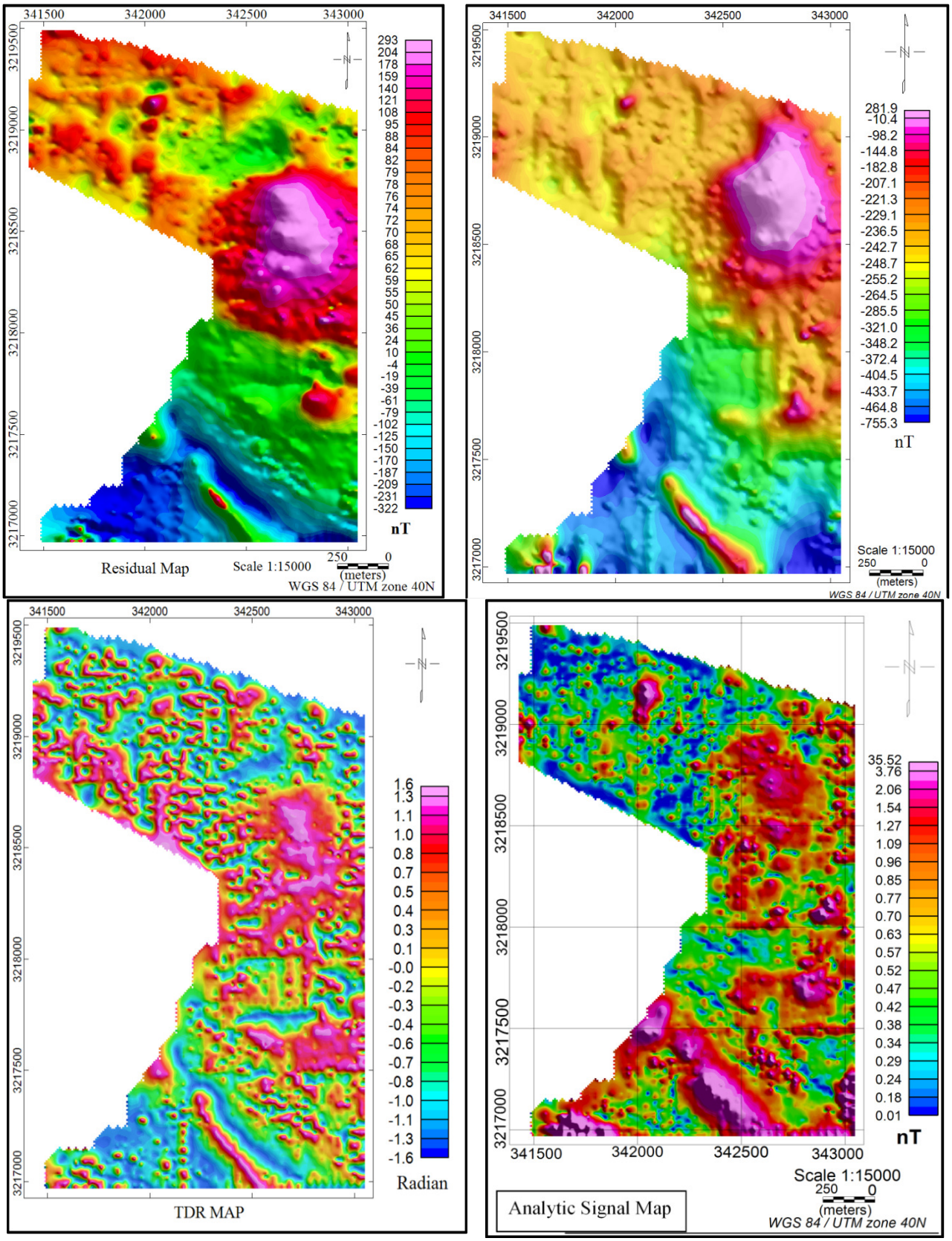

Figure-2 a) Residual magnetic field intensity map, b) reduction to magnetic pole map,c) Analytic signal map, d) Tilt derivative map (TDR).

Simple magnetic models follow the Euler equation, and the N is interpreted as the structure index, which is a criterion for the rate of field change with distance[2]. Equation (4) can be written as the following:

$$x_i \frac{\partial T(x_i+y_i+z_i)}{\partial x} + y_i \frac{\partial T(x_i+y_i+z_i)}{\partial y} + z_i \frac{\partial T(x_i+y_i+z_i)}{\partial z}$$

$$x_i \frac{\partial T(x_i+y_i+z_i)}{\partial x} + y_i \frac{\partial T(x_i+y_i+z_i)}{\partial y} + z_i \frac{\partial T(x_i+y_i+z_i)}{\partial z}$$

$$+NT(x_i + y_i + z_i) = x_0 \frac{\partial T(x_i+y_i+z_i)}{\partial x} + y_0 \frac{\partial T(x_i+y_i+z_i)}{\partial y} \quad (5)$$

$$+z_0 \frac{\partial T(x_i+y_i+z_i)}{\partial z} + NB$$

Where $T(x_i, y_i, z_i)$ is the measured data for the total field at points i = 1,2,3, ..., n. By choosing a window with appropriate widths on the data and moving this window over the network, this equation is solved for each window by the least squares method, and the parameters of the magnetic source for each window are obtained for a given structure index. The inversion process leads to an uncertainty for every fitted parameters which the uncertainty is used as the criteria for accepting or rejecting Euler equations. For magnetic data, the important advantage of the inversion process of the Euler equation is that the angles of the gradient, magnetic deviation, and magnetic residual component are not sensitive.

Several important items to obtain results in the Euler approach include: the correct choice of N, the Euler window size, and uncertainty of the depth[10].

Table-1: Structural indices for Euler deconvolution of magnetic anomalies[1,2,11].

Geologic Model	N
Horizontal contact	0
Vertical contact	0 - 0.5
Dyke/Sill	1
Vertical cylinder	2 - 2.25
Horizontal cylinder	2 – 2.75
Cylinder with unspecified stretch	2.5
Sphere	3

It should be noted that the minimum and maximum depth are equal to the size of the grid and, twice the size of the window, respectively. The advantages of this method regarding the magnetic data are that all calculations are independent of the angles of magnetic inclination and declination. The size of the window should be large enough to show the changes in a field, continuously. On the other hand, it should not be large enough to place several sources in a window[12].

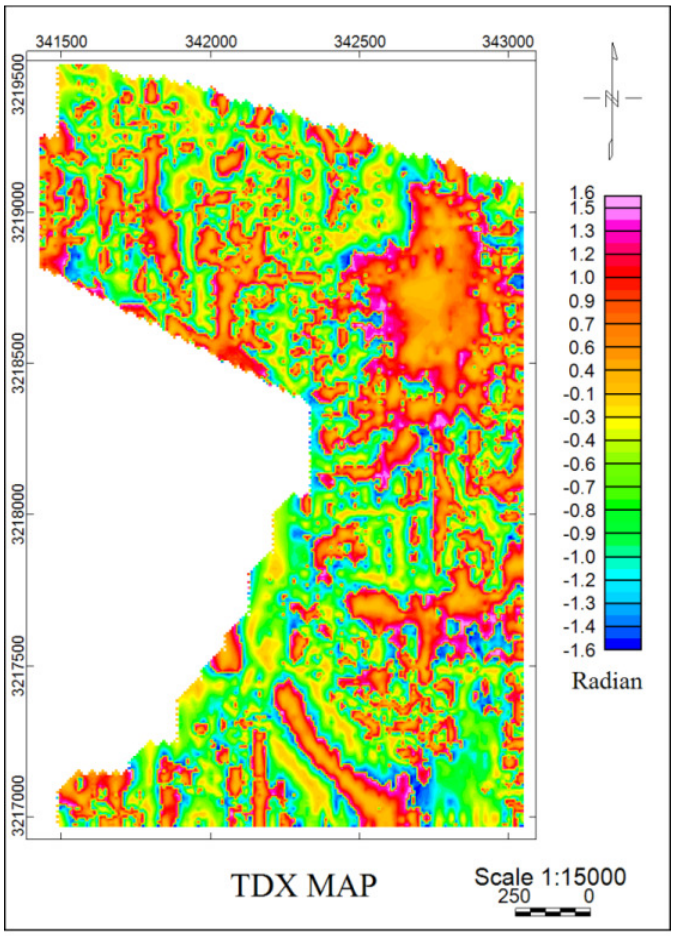

Figure-3: Total horizontal derivative (TDX) map.

Applying the Euler approach on synthetic data: To evaluate the accuracy and efficiency of Euler deconvolution method, it is necessary to apply this method to synthetic data. Using forward-mode modeling, the synthetic data are generated for thin two-dyke synthetic models. Then, the data reduced to the magnetic pole and the pseudo-gravity data, as well as the analytical signal, are calculated for this synthetic magnetic data.

The Euler method answers over the residual and reduced to the pole data (Figure-4d, e) are then compared with their actual values. Table-2 represents the characteristics of dyke synthetic models.

Figure-4a presents the grid of two dyke synthetic models, in which bipolar anomalies are well characterized. In Figure 4*b*, the map of the pseudo-gravity is provided. This map considers the dipole dyke as a monopole and shows the main anomalous position, which, according to the map (Figure-4*a*) and the

position of the dykes, the pseudo-gravity map provides the optimal results. Figure-4*c* shows an analytical signal map indicating an anomaly boundary to an acceptable degree.

Figure-4d represents the response of the Euler deconvolution method to the synthetic model residual map. For this purpose, different windows with different structural indices were investigated using the Euler method. The sizes of windows 4, 5, 6, 7, 8, 9, 10, 11 and 12 and the structural index of 1, 1.2 and 1.3 were applied. The error of depth estimation (standard deviation) was selected in the processing as 5%, 10% and 15% by the deconvolution method.

There are a lot of solutions in the various solutions list for different structural indexes that are far from our purpose, and the mask process must be applied in order to remove them, meaning that at each stage, a number of solutions with less accurate will be eliminated from the table of solution points. The conditions considered for limiting the solution points are x/ y-offset including the values between 70 and -70 m and dxy values between 0% and 30%. By mapping the solution points on the TMI map, we can examine the quality of the obtained data. The best set of solution points is a set where the point of the Euler deconvolution is not obtained, when the data are noisy, but without anomalies. After mapping the remaining points the best set of Euler solution points with a structural index of 1.3, a window size of 5, and a depth estimation error of 10% was determined after applying the mask process.

The residual points of the above conditions are depicted on the RTP map in Figure-4e. It is indicated from this map that the anomaly related to dyke 1 is in the depth of about 40 m, and the anomaly related to dyke 2 is in the depth of 60 m, which is confirmed by the real results of the models. Figure-4e shows the response of the Euler method on the RTP map, which this filter causes more symmetrical in terms of the shape of the magnetic anomaly and its analytical amplitude, and therefore the depth and structural index are calculated more accurately.

After transferring to the magnetic pole and using the structural index of 1.3 and window size of 5 provided the best answer for the synthetic models, which the anomaly related to a dyke 1 is in the depth of 40 m, and the related to the dyke 2 is in depth of 60 m, consistent with the actual model results. According to the results in the Figure 4*e*, the accuracy of the solutions is higher than the previous state.

Applying Euler deconvolution process on the actual data: The most important parameters required in the Euler deconvolution method are the SI and the window size, which should be selected carefully since Euler's method accuracy and precision depend on the exact selection of these two parameters. For this purpose, different windows with different structural indices were studied via Euler's method that the window size of 15 and the structural index of 1.3 provided the most appropriate response.

Table-2: Specifications of dyke model for synthetic data production.

Dyke Parameters	Parameters Size	
	Dyke 1	Dyke 2
Length (m)	200	250
Width (m)	5	8
Thickness (m)	30	30
Dip (°)	90	90
Azimuth (°)	40	90
Depth to the Top (m)	40	60
Magnetic susceptibility (SI unit)	0.07	0.08
Inclination (°)	46	46
Declination (°)	3	3

The error of estimation depth (standard deviation) was selected in the processing through deconvolution method by 5%, 10%, and 15%. In processing, it is indicated that increasing the window size and the structural index, the number of solution points increases, it can also be concluded that increasing the structural index in the same conditions, the window size and other limiting properties, the estimated depth increases, as well. The number of solutions obtained by the Euler method is provided for the windows of 5, 7, 10, 15 and 20 for the structural indices of 1, 1.3, and 1.6. After obtaining these solutions, the low-accuracy solutions should be removed from the solutions set. The solution points Table is provided considering the ideal state of the grid, ie the size of the grid cell was considered as a quarter to one-eighth of the distance between the survey lines, that is, 10 m. In applying the Euler deconvolution, the larger the anomalies in the grid, the larger window size should be considered to achieve more acceptable results in terms of the position of the more concentrated points on the shape including the trend of anomalies. However, the points do not have a good position on the map based on the considered cell size, the larger window size should be considered. If the optimal results are still not achieved, we should increase the size of the grid in different ways. The application of different conditions for the Euler process in this region showed that the best responses are obtained for the structural index of 1.3. In the Euler process, the resulting solution list contains several parameters including the window center coordinates (x and y), the depth, the percentage of the depth (dz) and surface uncertainties (dxy), and the distance between the solution points from the center of the window (x/ y-offset). The less the distance between the solution points from the center of the window, the more accurate the surface position

of the anomalies will be determined, and if these values are more than half the size of the Euler window, means that the solution point is placed outside the Euler window. There are numerous solutions in the various solution lists for different structural indexes that are far from our objective, and the mask process must be applied to eliminate them, indeed, at each stage, a number of less accurate solutions are eliminated from the solution points table. The conditions for limiting the resolution points are x/ y-offset values between 70 m and -70 m and dxy values between 0% and 30%.By mapping the solution points on the TMA map, we can examine the quality of the obtained data. The best set of solution points is a set that, in areas where noise data, but without anomalies exist, a solution point is not achieved from the Euler deconvolution. After mapping the remaining points the best set of Euler solution points were determined with a structural index of 1.3, the window size of 15 and a depth estimate of 10% after applying the mask process. Figure 5represents the points departing from the above conditions, on the residual map. It is indicated from this Figure that the anomaly center is in a depth of about 35 m and the northwest of anomaly in the depth of around 25 m, and the southeast part is in the depth of about 50 m.

Source Parameter Imaging (SPI): The current approach includes estimating the depth in the frequency domain based on phase changes (tilt angle in the boundary estimation field) of the potential field data, which is called source parameters imaging method. This method can work on three-dimensional data and its benefits are as the following: i. In this method, the map of the tilt angle is obtained from potential field data, the minimum of which is placed on the boundaries of the causative body. despite the second-order vertical derivative, there is no displacement between the minimum value and the body boundaries. ii. The results of this method do not depend on the parameters of the Earth magnetic field vector and also the magnetization vector of the body (angle of inclination and declination).

This method uses the analytic signal theory for the following reasons: i. An analytic signal function is defined for both the total field anomalies as well as for the horizontal component of the potential field. The first case is used to estimate the depth in the thin plate models, and the second one is used to estimate the depth in the sloping contact model. ii. The use of an analytical signal leads to boundary estimation without the need to know the characteristics of body magnetization.

Nabighian defined the analytic signal function as a mixed function, for which the real part is the horizontal derivative and the virtual part is the vertical derivative of the potential field data. He introduced two ways to calculate the analytical signal[13]: i. Calculating the derivatives of potential field data in different directions and combining them as a complex number with the described properties. ii. Using Hilbert transformation property between the derivatives of the potential field.

$$A(x,y) = |A|\exp(j\,\theta) \quad (6)$$

Where A is the domain of the complex number or the size of the analytical signal and J is the phase of the complex number (the title angle in the boundary estimation section) and are calculated from the following equations, respectively:

$$|A| = \sqrt{(\frac{\partial M}{\partial x})^2 + (\frac{\partial M}{\partial z})^2} \quad (7)$$

$$\theta = \tan^{-1}(\frac{\partial M}{\partial z} / \frac{\partial M}{\partial x}) \quad (8)$$

Atchuta Rao et al. employed the analytical signal size and phase angle to estimate the depth from two-dimensional profiles[13]. A further quantity called the local frequency, f is required to estimate the depth three-dimensionally, which is obtained from the following equation:

$$f = \frac{1}{2\pi}\frac{\partial}{\partial x}\tan^{-1}\left[\frac{\partial M}{\partial z} / \frac{\partial M}{\partial x}\right] \quad (9)$$

The local frequency, f, is defined as the rate of local phase change relative to the x and y-axes.

$$k = \frac{1}{|A|^2}\left(\frac{\partial^2 M}{\partial x z}\frac{\partial M}{\partial x} - \frac{\partial^2 M}{\partial x^2}\frac{\partial M}{\partial z}\right) \quad (10)$$

Using the above initial concepts, we can estimate the body parameters of the sloping contact model. If M represents the magnetic response of the sloping contact mass, then the M vertical and horizontal gradients are calculated from the following equations[4]:

$$\frac{\partial M}{\partial z} = 2KFc\sin d \times \frac{x\cos(2I-d-90) - h\sin(2I-d-90)}{h^2+x^2} \quad (11)$$

$$\frac{\partial M}{\partial x} = 2KFc\sin d \times \frac{h\cos(2I-d-90) - x\sin(2I-d-90)}{h^2+x^2} \quad (12)$$

K is the difference between the susceptibility of the body with the surrounding rocks, F is the magnitude of the surrounding magnetic field; $c = 1 - \cos^2 i \sin^2 \alpha$, α is the angle between the magnetic north and the axis x, i is the angle of inclination of the surrounding magnetic field; $\tan I = \tan i/\cos \alpha$, d is the slope of the contact model which is calculated from the positive direction of axis x and h is depth to the top of the body. All the angular quantities are measured in degrees. In the above relation, iis the angle of inclination of the magnetic field of the considered position, and it is completely independent of the body magnetization properties (angle of inclination of body magnetization). As a result, one of the advantages of this method is in the cases where no data is available regarding the residual magnetism of the body.

Replacing Eq (11) in the local wavelength relation, an equation is obtained in terms of the depth of the body and the variable x.

$$k = \frac{h}{h^2+x^2} \quad (12)$$

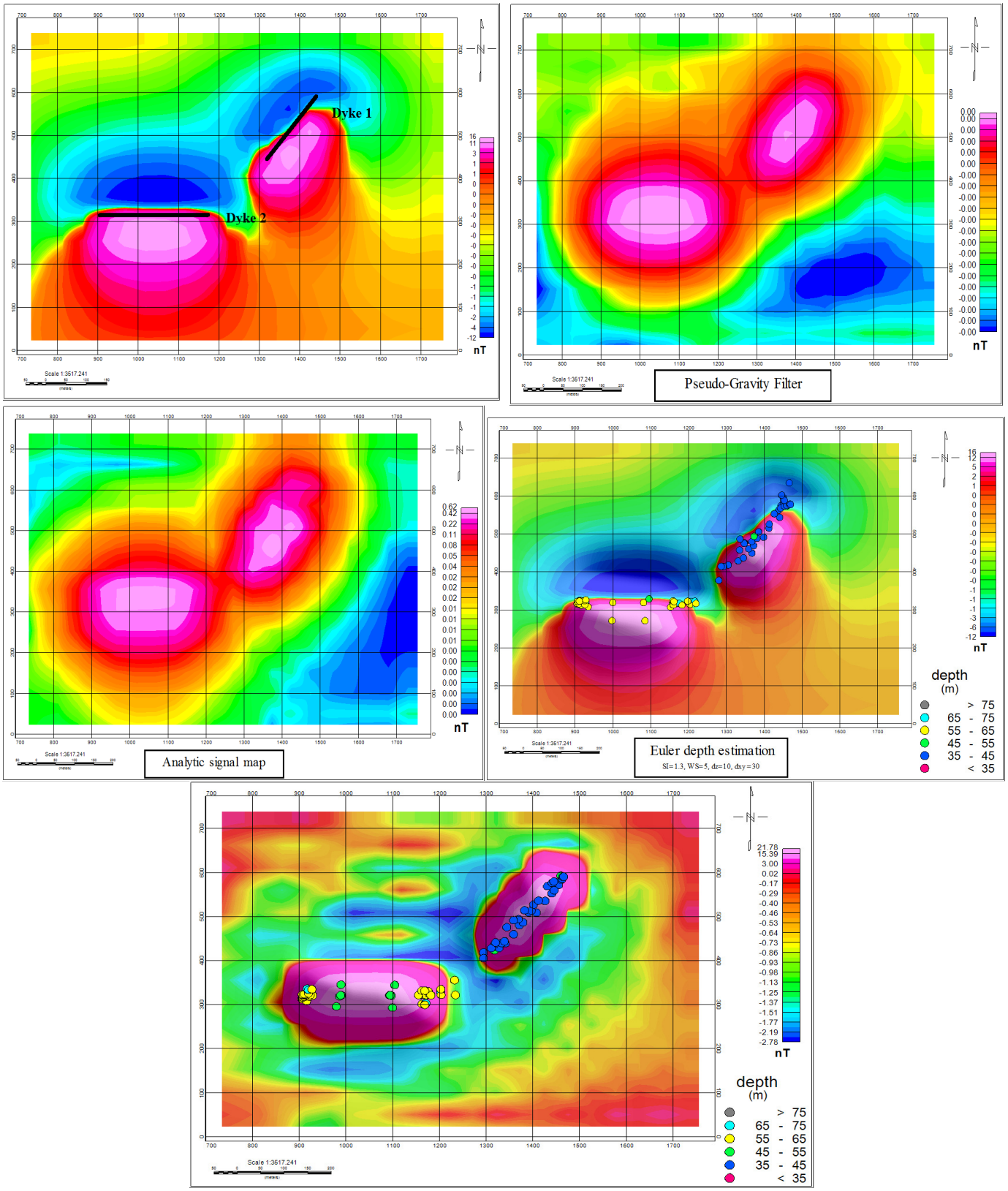

Figure-4: a) the magnetic gradient generated by the synthetic model (two thin dykes), b) the pseudo-gravity mapping of the map A, c) the analytical signal map of the map A, d) the Euler method response to the synthetic data, e) The divers map to pole and Euler method response on synthetic data after applying the diverse filter to the pole.

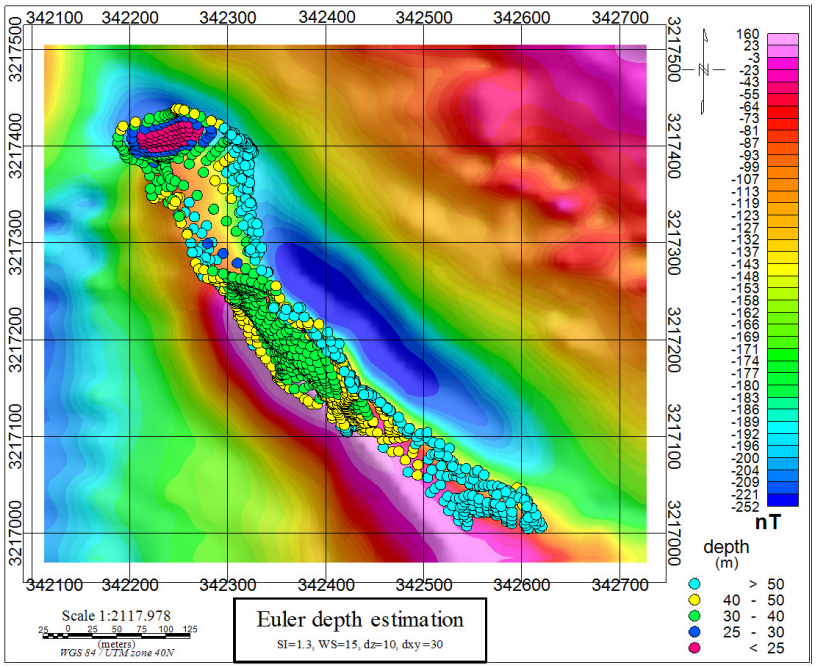

Figure-5: The results of the Euler deconvolution process on the RTP map.

The Eq.(12) shows that the maximum local wavelength does not depend on the inclination angle of the Earth magnetic field vector and the magnetization vector of the body. By choosing the coordinate system with the origin of x = 0, exactly above the edges of the body, one can calculate the depth to the top of the body as the following:

$$x = 0 \rightarrow k = \frac{1}{h} \rightarrow h = \frac{1}{k} \qquad (13)$$

To calculate the gradient of the body, we plot the different gradients of the body magnetic response in the phase angle relation, then, we have:

$$\theta = \tan^{-1}\frac{x\cos(2I-d-90)-h\sin(2I-d-90)}{h\cos(2I-d-90)+x\sin(2I-d-90)} \rightarrow \text{if} x = 0 \rightarrow \qquad (14)$$

$$\theta = \tan^{-1}\frac{-h\sin(2I-d-90)}{h\cos(2I-d-90)} = \tan^{-1}(-\tan^{-1}(2I-d-90)) =$$

$$-(2I-d-90) \rightarrow d = \theta + 2I - 90$$

Since the magnetic data are discrete, the horizontal gradient of the data can be calculated using the finite difference method. The calculation of vertical gradients is performed in the frequency domain using the Fourier transforms. After calculating the gradient of the data, the value of the phase angle is determined; therefore, the value of this quantity is known. With the value of the phase angle, the body slope can be determined using the Equation (14).

When applying the above relations, it is assumed to the minimum effect of the adjacent bodies. On the other hand, since second-order derivatives are applied in this method, the presence of adjacent bodies is negligible. It is also practical to estimate the body parameters on 3D data (grid). This has two advantages: First, through this, the possible error due to the non-perpendicularity of the body line on the survey line is eliminated. Secondly, contrary to the boundary estimation methods such as Euler, there is no limitation in selecting the window dimensions used in the estimation.

In practice, to apply this method to network data, the following steps are taken: i. Calculating the vertical derivative of the field data in the frequency domain. ii. Calculating the horizontal derivative of the data in the body direction. iii. Using the above formulas to reach the body parameters such as depth, slope, and difference of susceptibility coefficient.

Applying the method on the synthetic data: To investigate the applicability of the SPI technique in the interpretation of field anomalies, this method was applied to the synthetic data of a different two-dyke noisy model. To survey the effect of noise on the results of the above-mentioned method, a noise with the Gaussian distribution, a mean of 0 and a standard deviation of 0.2 was added to the magnetic data.

Table-2 provides the specifications of the models and these models are assumed without the residual magnetism. In Figure 6, the magnetic body response of the model and the results of the depth estimation with the SPI method are presented, indicated by colored circles. First, the SPI method was applied to the noisy models, which did not produce appropriate results. Therefore, to overcome this problem, we have to eliminate the noise. In practice, in order to avoid the impact of the depth estimation on the results, to eliminate the surface noise, the

noise reduction filters should be used such as the upward continuation filter. The height of the filter is equal to one-eighth to one-fourth of the distance between the magnetic surveying profiles, which was beyond 15m to these synthetic models. Considering the Figure-6, the depths of Dyke 1 and 2, is 40m and 60m, respectively, in average, which is equal to the actual depth of the magnetic body. The existence of noise in the data proves that, first, the results of the depths estimation are not obtained entirely at the boundary points of the body and are spatially distributed at points outside the body. Second, the estimated depth values are different from the real depth of the magnetic anomaly-producer body.

Applying the SPI process on the actual data: This method was also applied to the anomalous magnetic data of the study area. Due to Figure-7, this method defines the depth changes of the anomalous body between 25m and 55m in the Gol-e-Gohar Area 8 in different parts of the considered body.

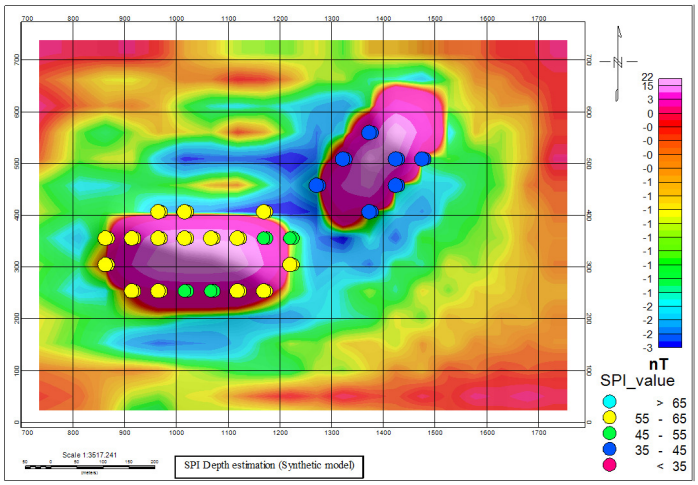

Figure-6: Application of the SPI method on unstructured synthetic magnetic data (after 15 m upward continuation).

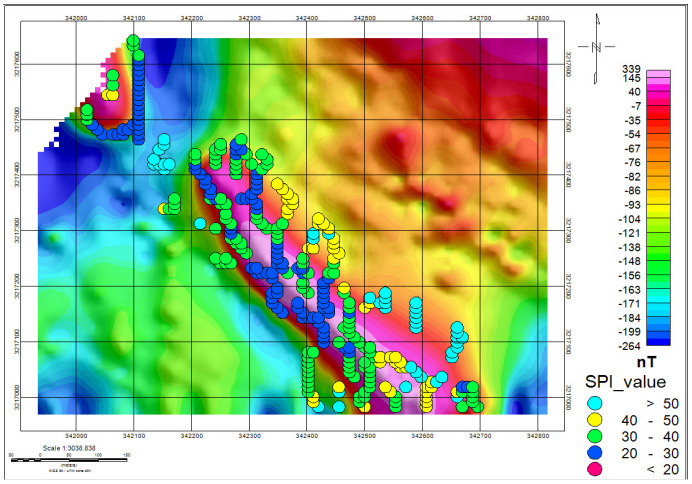

Figure-7: Application of the SPI method to actual magnetic data.

Werner deconvolution

The Werner deconvolution method is an automatic approach for analyzing the depth and the horizontal position of the gravity and magnetic data that is used along the profile and is very similar to the Euler method. Werner method is based on the assumption that magnetic anomalies can be estimated by thin and sheet-like plates such as dykes, sills, or geomagnetic compounds with the expansion of non-borders infinite depth. The dyke-related magnetic field equation with infinite longitudinal extension and wide depth is as the following[15]:

$$\Delta T(x) = \frac{A(x-x_0)+Bd}{(x-x_0)^2+d^2} \quad (15)$$

In the above relation, d is the depth of the dyke peak, B and A are constants that are functions of the magnetic field, susceptibility, and the geometric shape of the source. x_0 indicates the horizontal distance along the track for a point that is directly above the dyke peak. The effective factor in the solutions obtained by the Werner method is the window size and the criterion for accepting the responses is their being clustered. Each Werner deconvolution operation is referred to as a window in a section of the anomaly profile and may generate a single solution. That starts at the beginning of the profile using the smallest window size moving through the profile to the end. Then the window size is added as one unit and the entire profile is re-processed. Various parameters exist for controlling the number of solutions produced by Werner method, as the following: i. Window Minimum length, ii. Window Maximum Length, iii. Widow Expansion Increment, iv. Window Shift Increment.

The Werner deconvolution method does not provide validated solutions at a depth less than the input data gap or deeper than the window length.

Applying the SPI approach on the synthetic data: To evaluate the accuracy and efficiency of Werner's method, it is necessary to apply this method to synthetic data. Using a forward-mode modeling, the synthetic data was generated for two-dyke synthetic thin models whose magnetic grid was prepared. After applying the RTP filter, the Werner method was applied to it, which its response is indicated in the Figure-8. According to the Figure, the depth of the dyke1 is about 30m to 45m and the depth of dyke 2 is also about 60m on average, which, given the actual characteristics of the synthetic models, this method is very accurate.

Applying the Werner process to the actual data: This approach was also applied to the magnetic data of the study area. Before applying this method to the real data, first, the RTP filter was applied to eliminate the horizontal position error of the responses. Then Werner method was applied to the data, which resulted in around 2000 Werner solutions that should be clustered. For this purpose, the desired window size was 5×5, and at least 2 solutions per each cluster were applied. After this process, about 450 solutions were created, which were plotted

on the RTP map. According to the Figure 9, this method estimated the changes of the depth of the anomaly producer body of the Gol-e-Gohar 8 at various points of the body between 25m to 50m and 65m in the southeast anomalous corner.

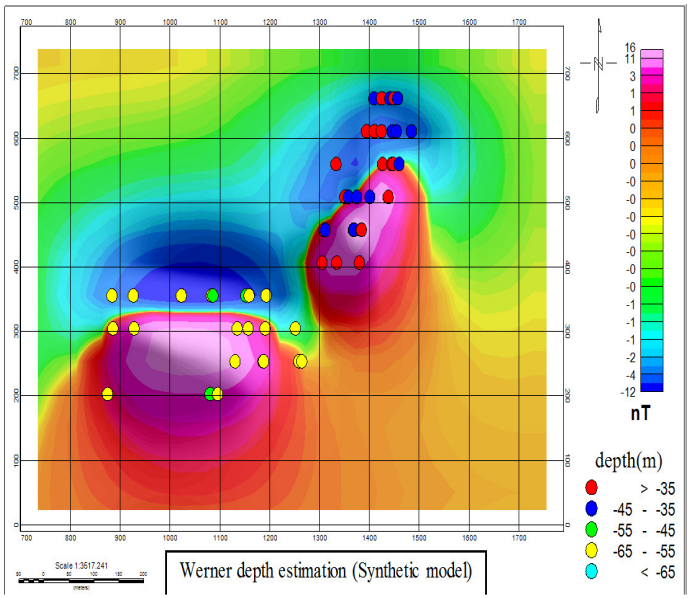

Figure-8: Werner Method on the synthetic magnetic data.

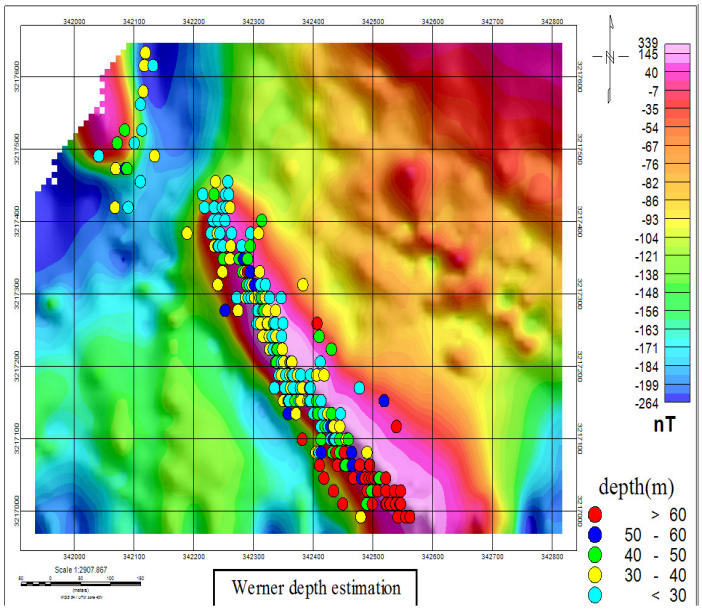

Figure-9: RTP map and applying Werner method to real magnetic data.

Potent Q: Interactive 2D modeling/inversion packages such as Potent allow definition of idealized magnetic source geometries in 2D or 2.5D sense. Modeling is based on fitting of the calculated model response to the observed magnetic response curves on profiles (ideally) perpendicular to the strike of anomalous structures.

The limitation is the use of rather simple model body shapes and general ambiguity in estimated parameters such as depth, width and susceptibility; especially for deeper sources (this limitation holds for all magnetic/gravity modeling and inversion in general). Because the 2D modeling is also very time demanding (as it needs a lot of interaction from the software user) we could not use 2D Potent modeling as a principal tool for depth estimation over the this project area. We used this method only to check against the results of other methods with the more global scope.

The results of the modeling from nine profiles (Figure-10) are summarized in Table-3. Figure-11. depicts the results of 4 profiles, the blue curves in Figure-11 (a, b, c, d) show the observed field values while the red curves show the calculated field values. The forward modeling being a trial and error technique, the shape, position, and physical properties of the model were adjusted in order to obtain a great correlation between the calculated field and the observed field data. Based on Figure 11and the results presented in Table 3, it is indicated that the depth over the body is 27 m in the north-west and 59 m in the south-eastern part of the structure, which is very close to the results of the depth estimation methods.

However, Forward modeling is also non-unique. Considering that the observed anomaly is ideal and has no specific complexity, so multiple models could fit our dataset (in instance dyke, lens, ellipsoid, and or sill). All magnetic anomalies are due to some form of magnetic mineral in the rocks.

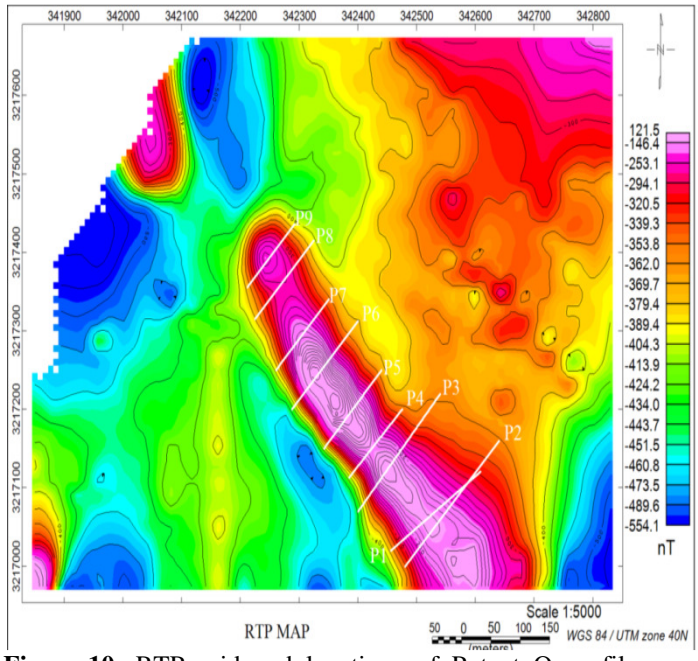

Figure-10: RTP grid and locations of Potent Q profiles are shown in white (P1 to P9).

Table-3: Results of 2D modeling.

Profile ID	Body type	Width (m)	Length (m)	Height (m)	Depth (m)	Strike (^{o})	Dip (^{o})	Plunge (^{o})	Susc (SI)
P1	Ellipsoid/ Lens	90	498	105	59	-35.4	14.3	-5	0.020
P2	Ellipsoid/ Lens	96	515	77	58	-44.2	14.3	-5	0.027
P3	Ellipsoid/ Lens	62	300	62	39	-46.2	13.7	4.2	0.053
P4	Ellipsoid/ Lens	82	510	45	28	-44.3	14.6	-3.8	0.029
P5	Ellipsoid/ Lens	92	500	58	28	-44.7	14.7	-4.0	0.026
P6	Ellipsoid/ Lens	58	515	57	30	-44.4	14.3	-3.9	0.037
P7	Ellipsoid/ Lens	88	332	46	32	-45.0	14.1	-4.9	0.095
P8	Ellipsoid/ Lens	115	335	36	27	-44.7	-3.3	-5	0.010
P9	Ellipsoid/ Lens	87	352	22	32	-45.0	14.9	-4.6	0.067

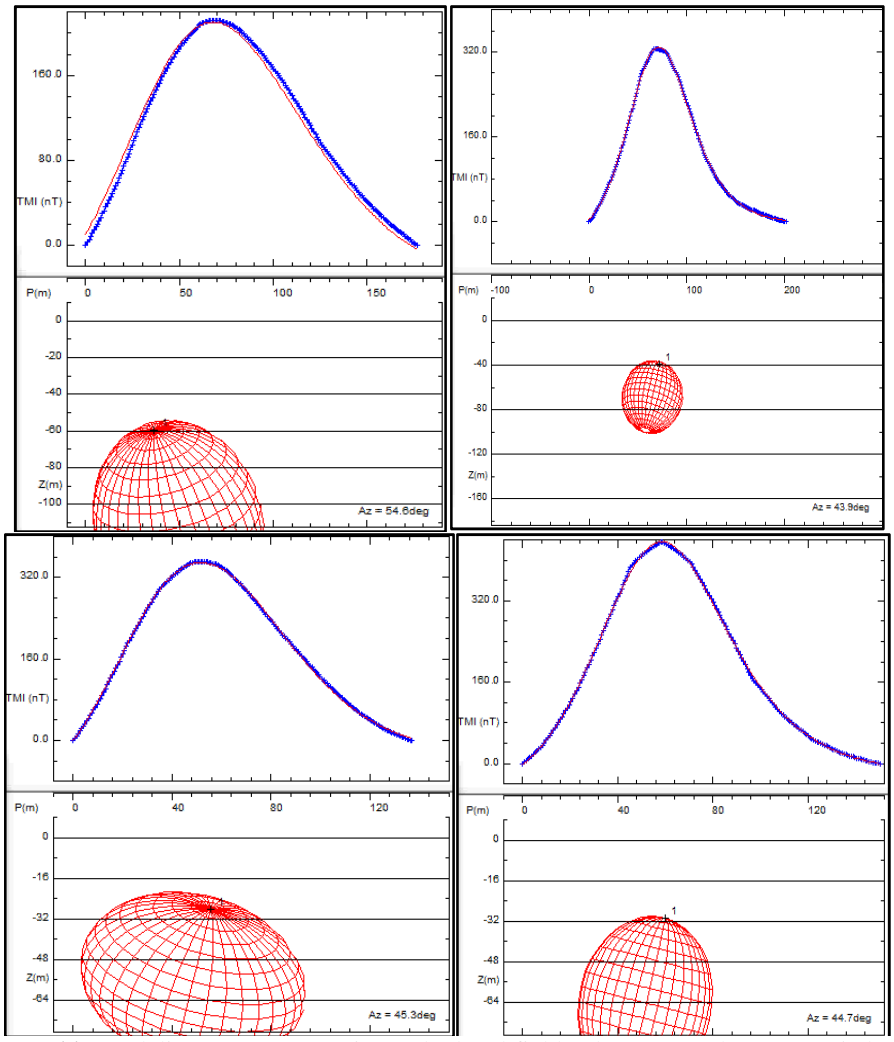

Figure-11: Modeling responses against calculated field values, a) P1, b) P3, c) P5, d) P6.

Conclusion

According to results of different maps and filters especially analytic signal, pseudo-gravity, horizontal and vertical derivative maps north anomaly with high extension as a monopole, is not very important. The related rocks containing magnetic minerals showed no iron mineralization with economic value. However, the southeast anomaly with the northwest-southeast trending is important for further exploration studies.

Considering the importance of the main anomalies in this area appearing as a dipole in the southeastern part, this anomaly is concentrated in this research, with three depth estimation methods and a two-dimensional modeling method applied to this anomaly, all four of which yielding relatively similar results. Before applying depth estimation methods on the real data, these methods were first examined on the synthetic models, which all the methods applied in this study are highly accurate. To estimate the edge of existing anomalies, in addition to the analytical signal and derivatives maps, TDR and TDX maps were prepared that clearly identify the edges of the anomalies in the study area.

Standard 3D-Euler deconvolution (ED) was applied on the RTP geomagnetic data. For different structural index and window size, different Euler 3Dsolution sets were generated. The reliable depth solutions are derived by using structural index 1.3 (dykeSI) window size of 15x15 and grid cell size 300m. The results of this method for estimating the depth of the ferromagnetic body depth indicated that the center of body is at a depth of about 35 m and northwest at the depth of about 25 m, and southeast parts of body are at the depth of about 50 m and higher.

SPI model was plotted on RTP map and the suitable depth estimate for the main anomaly determined. Based on the SPI method, at different points of the body, the depth is between 25 m and 55 m. Using Werner method, the depth variation in the different parts of the body is estimated to be between 25 m to 50 m in the various points of the body and about 65 m in the southeast corner.

After getting initial information about magnetic sources, the process of forward modeling and inversion are used. Potent Q, was applied to nine profiles across the southeast anomaly. The maximum determined RMS error for the observed to calculated responses was 3.5.

For the majority of the depths, the Euler solutions, SPI, Werner basement indicators, and also Potent models were within general agreement of each other. however, considering the results of synthetic models and the measured data, it is indicated that the three-dimensional Euler Deconvolution method is the most appropriate method for estimating the depth. It should be noted that the precision of the proposed techniques depends on the shape and the source of the anomaly. The more ideal and simple and not affected by several sources the mass form is, the more accurate the answer will be. Therefore, applying these methods on actual data, the depth to the top of anomaly is determined 35 m in the center and the northeast of the body and up to 50 m in the southeast part.

Acknowledgements

We thank the Iranian Mines & Mining Industries Development & Renovation (IMIDRO) for permission to use their data from the Gol-e-Gohar area and also Mojgostar Co. for providing us with the geophysical and geological data used in this work.

References

1. Thompson D.T. (1982). EULDPH: A new technique for making computer-assisted depth estimates from magnetic data. *Geophysics*, 47, 31-37.

2. Reid A.B., Allsop J.M., Granser H., Millett A.J. and Somerton I.W. (1990). Magnetic interpretation in three dimensions using Euler deconvolution. *Geophysics*, 55, 80-91.

3. Hansen R.O. and Simmonds M. (1993). Multiple source Werner deconvolution. *Geophysics*, 58, 1792-1800.

4. Thurston J.B. and Smith R.S. (1997). Automatic conversion of magnetic data to depth, dip, and susceptibility contrast using the SPI(TM) method. *Geophysics*, 62(3), 807-813.

5. Smith R.S., Thurston J.B., Dai T. and MacLeod I.N. (1998). ISPITM: The improved source parameter imaging method. *Geophys. Prosp*, 46, 141-151.

6. Nabatian Gh., Rastad E., Neubauer F., Honarmand M. and Ghaderi M. (2015). Iron and Fe–Mnmineralisation in Iran: implications for Tethyan metallogeny. *Australian Journal of Earth Sciences*, 62(2), 211-241.

7. Miller H.G. and Singh V. (1994). Potential Field Tilt – a new concept for location of potential field sources. *Journal of Applied Geophysics*, 32, 213-217.

8. Verduzco B., Fairhead J.D., Green C.M. and MacKenzie C. (2004). New insights into magnetic derivatives for structural mapping. *The Leading Edge*, 23(2), 116-119. doi:10.1190/1.1651454.

9. Cooper G.R.J. and Cowan D.R. (2006). Enhancing potential field data using filters based on the local phase. *Computers and Geosciences*, 32, 1585-1591.

10. Barbosa V.C.F., Silva J.B.C., Medeiros W.E. (2000). Making Euler deconvolution applicable to ground magnetic surveys. *J. Appl. Geophys*., 43, 55-68.

11. Whitehead N. and Musselman C. (2008). Montaj Gravity/Magnetic Interpretation: Processing, Analysis and Visualization System for 3D Inversion of Potential Field

Data for Oasis montaj v 6.3. Geosoft Incorporated, 85 Richmond St. W., Toronto, Ontario, M5H 2C9, Canada.

12. Blakely R.J. (1995). Potential theory in gravity and magnetic applications. Cambridge Univ. Press, United Kingdom, 1-441. ISBN: 0-521-57547-8

13. Nabighian M.N. (1972). The analytic signal of two-dimensional magnetic bodies with polygonal cross-section: Its properties and use for automated anomaly interpretation. *Geophysics*, 37(3), 507-517.

14. Rao D.A., Babu H.R. and Narayan P.S. (1981). Interpretation of magnetic anomalies due to dikes: The complex gradient method. *Geophysics*, 46(11), 1572-1578.

15. Pilkington M. and Todoeschuck J.P. (1993). Fractal magnetization of continental crust. *Geophysical Research Letters*, 20(7), 627-630.